

Electrical transport in passivated Pt/TiO₂/Ti Schottky diodes

Th. Dittrich^{a)}*Hahn-Meitner-Institut, Glienicker Strasse 100, D-14109 Berlin, Germany*

V. Zinchuk and V. Skryshevskyy

Department of Radiophysics, Taras Shevchenko University, Volodymyrska street 64, 01033 Kyiv, Ukraine

I. Urban

Bundesanstalt für Materialforschung, Unter den Eichen 87, D-12205 Berlin, Germany

O. Hilt

sglux Gesellschaft mit beschränkter Haftung (GmbH), Ostendstrasse 25, D-12459 Berlin, Germany

(Received 11 April 2005; accepted 14 October 2005; published online 18 November 2005)

Pt/TiO₂/Ti Schottky diodes were investigated by current-voltage analysis, photoresponse, and transient photocurrent (PC) in a wide temperature range. The compact TiO₂ as well as the SiO₂ passivation layers were prepared by the sol-gel technique. The Schottky-barrier height (1.2–1.3 eV) was equal to the difference of the work functions of Pt and Ti. The temperature dependence of the ideality factor was interpreted in terms of a Gaussian distribution of barrier heights [J. H. Werner and H. H. Güttler, *J. Appl. Phys.* **69**, 1522 (1991)]. Space-charge-limited currents under the presence of defects with an exponential distribution were observed. Under zero-potential condition, the PC transients were practically independent of temperature and the electron drift mobility amounted to 2×10^{-4} cm²/(V s). A screening dipole layer at the Pt/TiO₂ junction was formed under low forward and reverse potentials. Defects were generated under electron injection. © 2005 American Institute of Physics. [DOI: [10.1063/1.2135890](https://doi.org/10.1063/1.2135890)]

I. INTRODUCTION

Wide-band-gap semiconductors are of special interest for high-temperature electronics,¹ sensing of ultraviolet (UV) light,² or gas sensing.³ Usually, materials such as SiC or GaN are used. In the past, TiO₂ became of great interest for applications in sensors⁴ or injection solar cells.⁵ However, for electronic devices, one has to consider that injected charge may dramatically influence the defect structure of a metal oxide since electrons are important for the chemical equilibrium between oxidation and reduction.⁶ This effect is used, for example, in electrochromic metal oxides such as WO₃.⁷

Schottky diodes have been studied extensively in the past for a large variety of semiconductors.⁸ The barrier height is the most important characteristic for a Schottky diode. For ionic semiconductors, the barrier height depends strongly on the work function of the metal.⁸ For materials with high electronegativity difference as oxides or most of the sulfides,⁹ the barrier height depends linearly on the electronegativity or work function of the metal. TiO₂ is a wide-band-gap semiconductor [anatase, $E_g = 3.45$ eV;¹⁰ rutile, $E_g = 3.06$ eV (Ref. 11)] and Schottky diodes can be formed with Pt.¹² A value of the Schottky-barrier height of 1.7 eV of the Pt/nanoporous TiO₂ contact was published.¹²

Many problems concerning charge transport in TiO₂ thin films or porous TiO₂ layers and its electronic nature remain open. In this work, Pt/TiO₂/Ti Schottky diodes serve as a very sensitive device structure to study related problems. Besides the barrier height at the Pt/TiO₂ junction, electron injection into the TiO₂ and its impact on space-charge limita-

tion [space-charge-limited currents¹³ (SCLCs)] of the current as well as on the behavior of electronic states in the TiO₂ have been studied. In the used devices, the TiO₂ layer has been produced by highly cost effective low-temperature techniques such as the sol-gel method.¹⁴ A disadvantage of low-temperature processes is the high degree of structural disorder leading to a low electron drift mobility. For example, the electron drift mobility amounts to about 5×10^{-6} cm²/(V s) in nanoporous TiO₂.¹⁵

UV photodiodes with a very thin Pt front contact, a thin TiO₂ layer, and a Ti back contact are studied by the complex of current-voltage (*IV*) characteristics, spectral photoresponse, and transient photocurrent measurements. The Schottky barrier is formed at the Pt/TiO₂ interface. It will be shown, for example, that the Schottky-barrier height of the Pt/TiO₂/Ti diode is equal to the difference of the work functions of Pt [5.65 eV (Ref. 16)] and Ti [4.33 eV (Ref. 16)] and that the electron drift mobility amounts to 2×10^{-4} cm²/(V s). Furthermore, the ideality factor of the Schottky diode was analyzed on the basis of the model of Werner and Güttler in which a Gaussian distribution of barrier heights is assumed.¹⁷

II. EXPERIMENT

For all experiments, commercially available UV photodiodes of the type tw30sx (sglux GmbH) were used. The tw30sx Schottky diode consists of a Pt front contact (about 10 nm in thickness), a compact TiO₂ layer (thickness $L = 150$ nm), and a Ti back contact. The diode is placed on a glass substrate and the Ti back contact is connected to the

^{a)}Electronic mail: dittrich@hmi.de

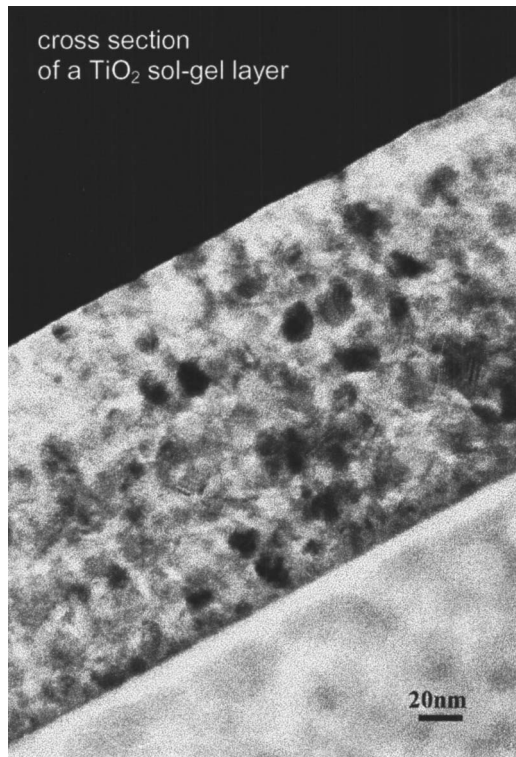


FIG. 1. Cross section of the active TiO₂ sol-gel layer.

metallic housing of the UV photodiode. The Ti and the Pt contacts were deposited with an electron-beam evaporator in high vacuum.

The TiO₂ active as well as the SiO₂ passivation layers were prepared by the sol-gel technique. A transmission electron microscopy (TEM) cross section of the TiO₂ layer is shown in Fig. 1. The compact TiO₂ layer was deposited in six steps of sol-gel dipping and each step can be identified by a very thin layer containing TiO₂ crystallites with a diameter of about 20 nm. It was shown by Raman spectroscopy that the TiO₂ consists predominantly of the amorphous and anatase phases. The final annealing step of the SiO₂ passivation layer was performed in air.

IV characteristics were measured with a Hewlett Packard 4140B picoampere meter. For photoresponse investigations in the spectral region from 0.4 to 4 eV, a quartz prism monochromator (SPM2) with a halogen lamp (150 W) was used. The light was chopped with a frequency of 8 Hz and the photoresponse was measured with an EG&G 5210 lock-in amplifier. The photoresponse spectra were normalized to the incident light intensity only, i.e., the change in reflectivity has not been taken into account. Photocurrent (PC) transients were excited with pulses of the third harmonic of a Nd:YAG (yttrium aluminum garnet) laser (wavelength 355 nm, duration time of a pulse 120 ps, EKSPLA SL312) of a relatively low energy (W) per pulse ($W_{\max} \leq 1 \mu\text{J}/\text{cm}^2$). The repetition rate of the laser pulses was 1 Hz and the PC transients were measured with a sampling oscilloscope (HP54510B). All measurements were carried out in a homemade cryostat allowing a variation of the temperature in a wide range (between -180 and $+300$ °C for the given conditions).

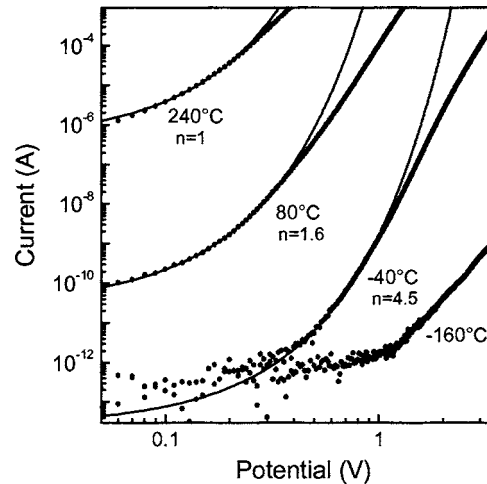


FIG. 2. Current-voltage characteristics of a tw30sx photodiode measured in forward direction at different temperatures (circles). The lines give the fits of the regions at lower potentials with the diode equation. Note the different ideality factors (n) at the different temperatures.

III. RESULTS AND DISCUSSION

A. Schottky-barrier analysis

Figure 2 shows the *IV* characteristics of the tw30sx photodiode measured in the forward direction at different temperatures. The *IV* characteristics are given in a log-log scale in order to get a better visualization of the processes involved. It may be noted that the rectification was better than three orders of magnitude, even at 240 °C, which makes these devices also interesting for applications at high temperatures. At lower potentials, the currents depend exponentially on the potential, which is typical for diodes. At potentials higher than a certain value V_x , the *IV* characteristics follow a power law. The power-law dependence of the current on the applied potential is a characteristic for space-charge limitation under the presence of traps with an exponential distribution.^{14,18} Therefore, two regions have to be considered separately for the analysis of the *IV* characteristics. The two regions are separated by a characteristic potential V_x which decreases with increasing temperature for T up to about 370 K and remains nearly constant around 0.2–0.3 V at higher temperatures. SCLCs will be analyzed in a separate section.

The solid lines in Fig. 2 give the fits of the regions at lower potentials with the diode equation

$$I = I_{\text{sat}} \left[\exp\left(\frac{qU}{nkT}\right) - 1 \right], \quad (1)$$

where I , U , I_{sat} , n , q , k , and T are the current, potential, saturation current, ideality factor, the elementary charge, the Boltzmann constant, and the temperature, respectively. In the case of the diffusion approach,⁸ one can write for I_{sat}

$$I_{\text{sat}} = f \frac{1}{T} \exp\left(-\frac{q\Phi_B}{kT}\right), \quad (2)$$

where f is a function of material parameters, such as dielectric constant, diffusion coefficient, and potential distribution. The value of the Schottky-barrier height Φ_B can be obtained

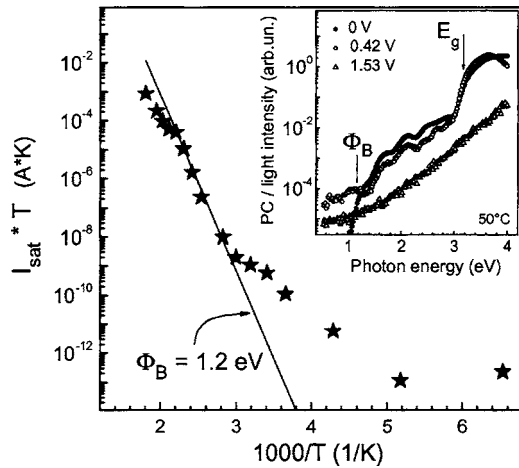


FIG. 3. Arrhenius plot of the saturation current multiplied with the temperature. The activation energy amounts to 1.2 eV in a wide region. The insert shows the spectral response of a tw30sx photodiode measured at 50 °C for different potentials in the forward direction.

from the Arrhenius plot of the product of I_{sat} and T . This is shown in Fig. 3. The activation energy is not a constant over the whole temperature range. This means that, under certain conditions, the Schottky-barrier height can be masked by the thermal activation of other processes such as transport. Nevertheless, a maximal activation energy of 1.3 eV holds at intermediate temperatures over about four orders of magnitude and has to be attributed to the Schottky-barrier height.

The Schottky-barrier height was obtained also from photoresponse measurements, i.e., from the internal photoemission of electrons from the very thin Pt front contact into the conduction band of the TiO_2 layer. In such a case, the measured photoresponse R is approximately⁸

$$\sqrt{R} \approx (h\nu - q\Phi_B), \quad (3)$$

where $h\nu$ is the photon energy. The filled circles of the insert of Fig. 3 show the logarithmic plot of the photoresponse of the Pt/ TiO_2 Schottky contact for zero-bias condition at 50 °C. The band gap (E_g) with the exponential tails below the band gap of the TiO_2 is clearly indicated by the steep increase of the photoresponse around 3.0 eV ($E_g \sim 3.2$ eV). A similarly steep increase can be seen around 1.1 eV. This part of the photoresponse is related to the photoemission of electrons over a barrier of about 1.2–1.3 eV. It should be pointed out that the internal photoemission limits the so-called visible blindness of the Pt/ TiO_2 Schottky diode in general.

The value of the Schottky-barrier height $\Phi_B \sim 1.2$ –1.3 eV obtained in our experiments agrees very well with the difference of the metal work functions of Pt and Ti. Further, it is significantly less than the value for the Pt/por- TiO_2 Schottky diode on a SnO_2 :F substrate [$\Phi_B = 1.7$ eV (Ref. 12)]. The morphology as well as the presence of TiO_2 and gaseous phases greatly influence the characteristics of the Pt/por- TiO_2 Schottky diode.

For the IV characteristics given in Fig. 2, the ideality factors of the Schottky diodes change strongly with temperature from 1.0 (at 240 °C) to 4.5 (at –40 °C). According to Werner and Güttler,¹⁷ the value of $n^{-1} - 1$ can be plotted as a

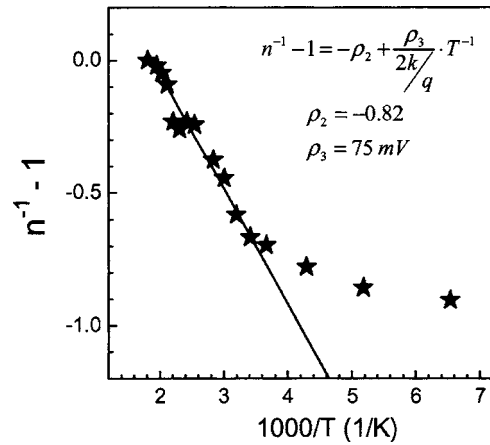


FIG. 4. Dependence of the ideality factor in the form of $n^{-1} - 1$ on the inverse temperature (stars). The solid line represents the fit at the higher temperatures.

function of the inverse temperature. This plot is shown in Fig. 4. At higher temperatures, $n^{-1} - 1$ depends linearly on $1/T$ while $n^{-1} - 1$ tends to saturate at lower temperatures. Werner and Güttler proposed a model in which the ideality factor can be described by a Gaussian barrier distribution.¹⁷ In this model, the parameters ρ_2 and ρ_3 (using the same symbols as in the original work) describe the potential-dependent change of the mean value of the barrier and of the standard deviation, respectively,

$$n^{-1} - 1 = -\rho_2 + \frac{\rho_3}{2k} T^{-1}. \quad (4)$$

Equation (4) followed from the fact that a voltage-independent ideality requires a linear increase of the barrier height. At the higher temperatures, the $n^{-1} - 1$ can be well fitted by Eq. (4) with $\rho_2 = -0.82$ mV and $\rho_3 = 75$ mV. These values are quite large in comparison to Schottky barriers of conventional semiconductors.¹⁷ The reason for these large values is related to a high density of electronic states in the exponential tails at the Pt/ TiO_2 junction.

B. Analysis of space-charge-limited currents

As mentioned above, the IV characteristics follow a power law at the higher potentials. In Fig. 2, the exponents are 6, 11, 8, and 5 for the temperatures of –160, –40, 80, and 240 °C, respectively. The exponents suggest SCLCs in the presence of traps with an exponential distribution. The power law can be written as¹⁸

$$I \approx q\mu N_c \left(\frac{\varepsilon\varepsilon_0}{qN_0 kT_i} \right)^l \frac{U^{l+1}}{L^{2l+1}}, \quad (5)$$

where μ , N_c , N_0 , ε , and kT are the electron mobility, the density of states at the conduction band, the trap concentration, the relative dielectric constant, and the characteristic energy of the exponential trap distribution, respectively, and $\varepsilon_0 = 8.85 \times 10^{-12}$ A s/V m. The exponential trap distribution is given by

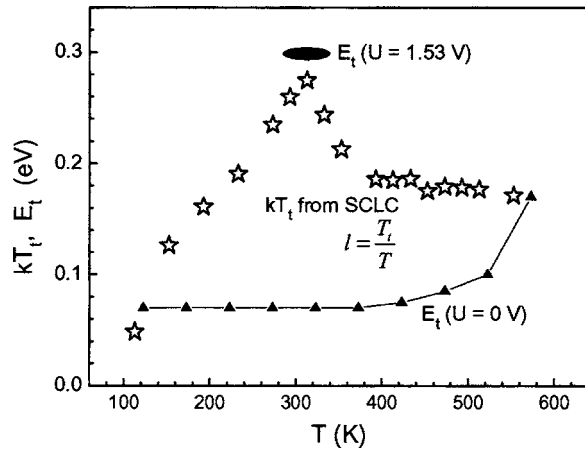


FIG. 5. Temperature dependence of the exponential tail (E_t) near the band gap (triangles) and of the kT_t parameter (stars), which corresponds also to an exponential defect distribution. The values of E_t and kT_t were obtained from the photoresponse and analysis of the SCLCs, respectively.

$$N_t(E) = N_0 \exp\left(\frac{E - E_c}{kT_t}\right), \quad (6)$$

where E and E_c are the energy and the edge of the conduction band. The power coefficient l is determined as the ratio between T_t and T ,

$$l = \frac{T_t}{T}. \quad (7)$$

Figure 5 shows the temperature dependence of the values of kT_t (stars). The values of kT_t increase with temperature from 50 meV (at 110 K) to 280 meV (at 310 K). Between ~ 310 and ~ 370 K, kT_t decreases from 180 to 170 meV and remains nearly constant with a further increase of T .

The values of kT_t obtained from the SCLC analysis can be compared with the characteristic energy of the exponential tails obtained from the photoresponse measurements (E_t) since both values are related to electronic defect states close to the band gap. Figure 5 depicts also the temperature dependence of E_t under noninjecting condition (triangles). Under zero-bias condition, the values of E_t are independent of the temperature ($E_t = 70\text{--}75$ meV) up to about 400 K. Above 500 K, E_t increases strongly up to 170 meV at 573 K. Surprisingly, the values of kT_t and $E_t(U=0$ V) are nearly equal only at the very low and very high temperatures. At the intermediate temperatures, the values of kT_t and $E_t(U=0$ V) may be very different. Under strong injection, the photoresponse spectra may change dramatically as demonstrated in the insert of Fig. 3 for $U=1.53$ V at 50 °C. In this case, one exponential spectrum with $E_t(U=0$ V)=300 meV has been formed over the whole investigated spectral range. The value of $E_t(U=0$ V)=300 meV is even larger than the maximal value of kT_t and may be considered as an upper limit for electronic defects with an exponential distribution in TiO_2 .

The strong increase of E_t and the decrease of the overall photoresponse under strong injection as well as the temperature dependence of kT_t are related to the formation of additional disorder accompanied by increased recombination due to the defect formation. The formation of additional disorder or defects under strong electron injection is not very surpris-

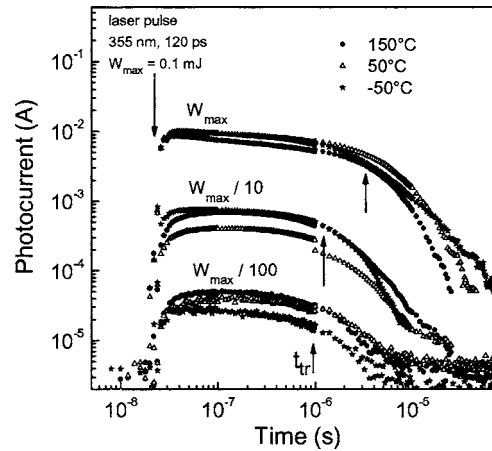


FIG. 6. Transient photocurrents measured at different temperatures and excitation intensities under zero-bias condition. The arrows mark the transit times.

ing since electrons participate generally in the chemical equilibrium of metal oxides as mentioned above.⁶ For example, trapping of electrons at Ti^{4+} changes the oxidation state to Ti^{3+} and therefore the whole chemical environment around the trapped electron. Under the presence of injected electrons, thermal activation of reactions leading to both formation and healing of defects has to be taken into account.

C. Photocurrent transients

In equilibrium, i.e., for $U=0$ V, a homogeneous electrical field can be assumed in the compact TiO_2 layer. The value of the electrical field is given by the TiO_2 thickness L and by the difference of the work function of Pt and Ti ($\Delta U=1.3$ V) and amounts to about 10^5 V/cm. Therefore, PC transients can be measured in a time-of-flight (TOF) regime for TiO_2 under equilibrium conditions as well as under applied potential. For a homogeneous field, the electron drift mobility can be obtained from the transit time (t_{tr}) by the following expression:¹⁹

$$\mu = \frac{L^2}{t_{tr}\Delta U}. \quad (8)$$

Figure 6 shows the PC transients measured at different temperatures and excitation intensity under zero-bias condition. For the given light intensities, the dynamic regime of the SCLCs is not reached. The PC transients decay by one to two orders of magnitude within 1–10 μs . The PC transients are practically independent of the temperature up to about 200 °C for low excitation intensity. Further, the PC transients show a well-pronounced plateau until they decay. This gives evidence for predominantly nondispersive transport. At high excitation intensity and higher temperatures, the transport becomes slightly dispersive, as can be indicated from the power-law dependence of the PC transient at times less than t_{tr} .¹⁹

The transit time is not exactly defined since the experiment has not been carried out under strong light absorption condition. The value of t_{tr} was determined from the time at the kink position of the PC transients. The values of t_{tr} increased with increasing power, W . The reason for this is an

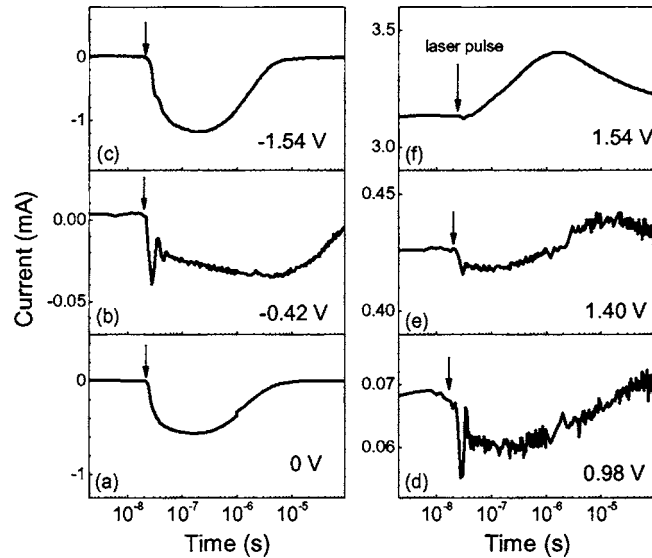


FIG. 7. Transient photocurrents measured at 50 °C for different potentials (0, -0.42, -1.54, 0.98, 1.4, and 1.54 V [(a)–(f)] respectively). The arrows mark the onset of the laser pulse.

increasing disturbance of the electrical field by trapped excess charge carriers, which cannot be extracted from the TiO₂ within 1 s (the repetition rate of the light pulses is 1 Hz). At low excitation intensity, the value of the electron drift mobility amounts to about $\mu=2 \times 10^{-4}$ cm²/(V s). This value is larger by more than one order of magnitude than for nanoporous TiO₂ (Ref. 15) but it is much smaller than the electron mobility in anatase-sputtered layers [4 cm²/(V s) at room temperature²⁰] or rutile crystals [of the order of 0.25 cm²/(V s) Ref. 21].

Figure 7 shows some PC transients measured at 50 °C for different potentials in reverse and forward directions. Under reverse bias, the electrical field is expected to increase with increasing potential. However, as can be seen from Fig. 7(b), the transit time increased (!) by about one order of magnitude at -0.42 V. This was also the case at even much smaller values of reverse bias. Additionally, the amplitude of the PC transients decreased by about one order of magnitude. Since there is no physical reason to assume a strong reduction of the electron drift mobility under respective conditions, the decrease of the transit time can be explained only by a decrease of the electrical field over the thickness of the TiO₂ layer, i.e., by partial screening of the electrical field in a narrow region close to the Pt/TiO₂ contact. At higher reverse potential [Fig. 7(c)], the transit time becomes shorter again and the amplitude of the PC transients increases.

The PC transients became longer and the amplitude smaller at low forward potential since the electrical field decreased [Fig. 7(d)]. Under injection, an electrical field with an opposite sign is created beginning from the injecting Ti contact. The distribution of this electrical field is determined by the injected electrons. The sign of the PC transients started to change at the longer times around $U=1$ V [Fig. 7(e)]. The different components within one PC transient demonstrate the nonhomogeneous field distribution in the TiO₂ layer. Under strong injection, the PC transients changed completely to a positive sign [Fig. 7(f)]. The offset of the PC

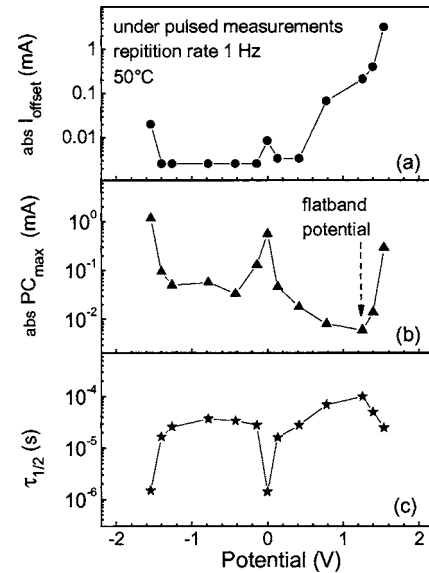


FIG. 8. Potential dependence of the offset current (a), of the absolute value of the photocurrent maximum (b), and of the time at the half maximum (c). At the higher potentials in forward direction, the value of $\tau_{1/2}$ was determined for the positive part of the photocurrent.

transients increases strongly and is significantly larger than the amplitude of the PC transients under strong injection. Therefore, the distribution of the electrical field is only slightly affected by the photoinjected excess charge carriers under strong injection.

Figure 8 summarizes the dependencies on the potential of the offset current (I_{offset}), the absolute value of the PC amplitude (PC_{max}), and of the time at which the PC transients decayed to $\frac{1}{2}(\tau_{1/2})$.²² At zero potential, I_{offset} and PC_{max} show a pronounced peak, while $\tau_{1/2}$ exhibits a sharp drop by 20 times in comparison to even very low reverse and forward potentials. Therefore, the electrical field decreased by about 20 times in the compact TiO₂ layer under nonequilibrium conditions. This is caused by the fact that the electrical field is mostly screened in the contact region by the formation of an additional dipole layer. The formation of a dipole layer at the Pt/TiO₂ interface under nonequilibrium conditions is caused by charge exchange at the Schottky barrier with defect states at the TiO₂ side. Under injection, I_{offset} increases strongly while PC_{max} decreases and $\tau_{1/2}$ increases with increasing U for U up to 1.2–1.3 V, which corresponds to the flatband potential. Under strong injection, the electrical field increases with increasing injection current which leads to the observed increase of PC_{max} and to the decrease of $\tau_{1/2}$.

IV. CONCLUSIONS

A photoelectronic device based on the Pt/TiO₂/Ti Schottky diode was studied by a complex of electrical and photoelectrical methods. The Schottky-barrier height was obtained from IV characteristics (activation of the saturation current), spectral photoresponse measurements (onset of photoemission from Pt into TiO₂), and PC photocurrents (flatband potential) and Φ_B amounts to 1.2–1.3 eV. Since this value corresponds to the work-function difference between Pt and Ti, it can be concluded that the barrier at the

TiO₂/Ti contact can be neglected and the electric field extends over the whole TiO₂ layer under equilibrium conditions. Under already slightly nonequilibrium conditions, an additional dipole layer is formed at the Pt/TiO₂ interface. This dipole layer screens the electrical field in the TiO₂ compact layer. The formation of the dipole layer should have also a great impact on the distribution of barrier heights, i.e., on the temperature dependence of the ideality factor. However, further detailed investigations are needed to get a deeper understanding about the formation of the barrier at the Pt/TiO₂ contact, especially with respect to the generation of defect states under nonequilibrium conditions. Further, space-charge-limited currents have to be considered already at relatively low potentials in the forward direction. For operation of Pt/TiO₂/Ti Schottky diodes under high electron injection or at very high temperatures, one has to take into account the generation of defects. This limits strictly the operation mode of related UV photodiodes. The electron drift mobility is quite low in the compact TiO₂ layer [of the order of 10⁻⁴ cm²/(V s)] which gives the principal limitation of the time response of electronic devices based on TiO₂ prepared by the given sol-gel technology.

ACKNOWLEDGMENT

The authors are grateful to the BMBF of Germany for financial support (UKR 01/062).

- ¹P. G. Neudeck, R. S. Okojie, and L.-Y. Chen, Proc. IEEE **90**, 1065 (2002).
- ²E. Monroy, F. Omnès, and F. Calle, Semicond. Sci. Technol. **18**, R33 (2003).
- ³See, for example, J. Schalwig, G. Müller, U. Karrer, M. Eickhoff, O. Ambacher, M. Stutzmann, L. Görgens, and G. Dollinger, Appl. Phys. Lett. **80**, 1222 (2002).
- ⁴See, for example, W. Göpel and G. Reinhardt, in *Sensors Update*, edited by H. Baltes, W. Göpel, and J. Hesse (VCH, Weinheim, 1996).
- ⁵M. Grätzel, Nature (London) **414**, 338 (2001), and references therein.
- ⁶See, for example, J. Rudolph, Z. Naturforsch. A **33**, 757 (1959).
- ⁷See, for example, N. Sharma, N. Deepa, P. Varshney, and A. A. Agnihotr, J. Sol-Gel Sci. Technol. **18**, 167 (2000).
- ⁸S. M. Sze, *Physics of Semiconductor Devices* (Wiley, New York, 1981).
- ⁹S. Kurtin, T. C. McGill, and C. A. Mead, Phys. Rev. Lett. **22**, 1433 (1969).
- ¹⁰H. Tang, F. Lévy, H. Berger, and P. E. Schmid, Phys. Rev. B **52**, 7771 (1995).
- ¹¹D. C. Cronemeyer, Phys. Rev. **87**, 876 (1952).
- ¹²R. Könenkamp, Phys. Rev. B **61**, 11057 (2000).
- ¹³A. Rose, Phys. Rev. **97**, 1538 (1955).
- ¹⁴C. F. Brinker and G. W. Scherer, *Sol-Gel Science* (Academic, Boston, 1990).
- ¹⁵V. Kytin and Th. Dittrich, Phys. Status Solidi A **185**, 461 (2001).
- ¹⁶H. B. Michaelson, IBM J. Res. Dev. **22**, 72 (1978).
- ¹⁷J. H. Werner and H. H. Güttler, J. Appl. Phys. **69**, 1522 (1991).
- ¹⁸M. A. Lampert and P. Mark, *Current Injection in Solids* (Academic, New York, 1970).
- ¹⁹See for more details, for example, W. E. Spear, J. Non-Cryst. Solids **1**, 197 (1969).
- ²⁰H. Tang, K. Prasad, R. Sanjines, P. E. Schmid, and F. Lévy, J. Appl. Phys. **75**, 2042 (1994).
- ²¹R. G. Breckenridge and W. R. Hosler, Phys. Rev. **91**, 793 (1953).
- ²²The time $\tau_{1/2}$ has been chosen instead of t_{tr} since $\tau_{1/2}$ is better defined for the different shapes of the PC transients.